

Potential of multiple injection strategies implementing the after shot and optimized with the design of experiments procedure to improve diesel engine emissions and performance

Original

Potential of multiple injection strategies implementing the after shot and optimized with the design of experiments procedure to improve diesel engine emissions and performance / D'Ambrosio, Stefano; Ferrari, Alessandro. - In: APPLIED ENERGY. - ISSN 0306-2619. - 155:(2015), pp. 933-946. [10.1016/j.apenergy.2015.05.124]

Availability:

This version is available at: 11583/2628091 since: 2016-01-13T17:15:04Z

Publisher:

Elsevier

Published

DOI:10.1016/j.apenergy.2015.05.124

Terms of use:

This article is made available under terms and conditions as specified in the corresponding bibliographic description in the repository

Publisher copyright

Elsevier postprint/Author's Accepted Manuscript

© 2015. This manuscript version is made available under the CC-BY-NC-ND 4.0 license
<http://creativecommons.org/licenses/by-nc-nd/4.0/>. The final authenticated version is available online at:
<http://dx.doi.org/10.1016/j.apenergy.2015.05.124>

(Article begins on next page)

1 **POTENTIAL OF MULTIPLE INJECTION STRATEGIES IMPLEMENTING THE AFTER SHOT**
2 **AND OPTIMIZED WITH THE DESIGN OF EXPERIMENTS PROCEDURE TO IMPROVE**
3 **DIESEL ENGINE EMISSIONS AND PERFORMANCE.**

4 *d'Ambrosio, S., and Ferrari, A.**

5 *Energy Department – Politecnico di Torino*

6 *C.so duca degli Abruzzi, 24, 10129, Torino, Italy.*

7 **1. ABSTRACT.**

8 The potential of the after-injection versus engine-out emissions, combustion noise and brake specific fuel consumption
9 has been evaluated for a Euro 5 diesel engine with a reduced compression ratio (16.3:1). The engine has been fueled
10 with conventional diesel fuel. In particular, the effects of injection strategies that feature either pilot and after-injection
11 shots, or double-pilot and single-after injection shots, have been assessed experimentally, in the presence of high *EGR*
12 fractions. Calibrations with triple and quadruple injection schedules have been optimized by means of a design of
13 experiments procedure. The performance of the thus calibrated propulsion system has been compared with data from a
14 previously optimized double injection schedule, characterized by a retarded main injection timing in order to intensify
15 the premixed combustion. The experimental data refer to different steady-state working conditions that are
16 representative of passenger car engine applications over the European homologation cycle. In-cylinder analyses of the
17 pressure, heat release rate, temperature and emissions have been performed in order to have a better understanding of
18 the effects of the implemented injection strategies on engine performance.

19 The substitution of the pilot- main injection schedule in the higher part-load zone of the *NEDC* region with a triple
20 injection, featuring both pilot and after shots, has led to lower NO_x and higher soot, while fuel consumption remains
21 almost the same. In general, the *EGR* trade-off soot- NO_x , $bsfc$ - NO_x , HC - NO_x and CO - NO_x curves do not change to any
22 significant extent when an after shot is added to the pilot-main injection train. Reductions in the combustion noise,
23 which depend on the changes in the pilot injection parameters that result from the design of experiments procedure, can
24 also be obtained, as a consequence of the addition of the after-injection to the pilot-main injection schedule. Pilot-pilot-
25 main-after strategies guarantee improved NO_x -soot and $bsfc$ - NO_x *EGR* trade-off curves at medium to high loads and at

* Corresponding author e-mail address: alessandro.ferrari@polito.it.

low to medium speeds, compared to both pilot-pilot-main and pilot-main-after strategies, and allow combustion noise to be diminished significantly.

Keywords: after injection; design of experiments; partial premixed charge compression ignition engines.

Highlights:

- The benefits of after injections are evaluated in a low-compression ratio Euro 5 diesel engine.
- Triple and quadruple injection schedules are compared with pilot-main and pilot-pilot-main strategies.
- The potential of after injections is examined in the higher part of the *NEDC* load zone.

2. INTRODUCTION

The fuel injection strategy can play an important role in simultaneously reducing passenger car diesel engine emissions [1, 2, 3, 4] and combustion noise [5], without neglecting fuel consumption targets. In other words, a multiple injection strategy, adopted to replace a single fuel injection shot with multiple discrete fuel injection events of reduced size, can easily be implemented using Common Rail (*CR*) systems, equipped with the modern injectors [6, 7]. These injectors can control small injected fuel quantities, despite pressure waves, and guarantee superior flexibility in the management of the dwell time, in order to fulfil Euro 5 and Euro 6 standards.

There are two primary multiple injection modes: the first elemental mode, which uses pilot injection, can be implemented by injecting an amount of fuel prior to the main injection (the pilot injected mass is small in conventional diesel combustion systems, but can also be significant in low temperature combustion strategies [2]), while the other employs after-injection, which consists of a small amount of fuel being injected separately, at the end of the main injection. The benefits and effects of pilot injections on emissions, combustion noise (*CN*) and fuel consumption have been evaluated and discussed in [8]. The focus of this work is on the exploitation of optimized after-injection in multiple injection strategies, in order to improve engine out emissions and in-cylinder performance. From this point of view, after-injection is efficient in reducing the soot engine-out emissions [9], which can be up to 40% lower than in the single injection case [10]. In general, after-injections can oxidize part of the unburned fuel and a decrease in *CO*, *HC* and *PM* engine-out emissions is obtained [11]. The benefits increase when mixing is difficult, i.e. at medium to high loads and under high *EGR* conditions when the utilization of in-cylinder air is critical [12, 13].

After-injections have also been proposed as a means of reducing turbocharger lag during engine transients, since the pressure and the temperature of the exhaust gas leaving the cylinder can be raised significantly [14]. This makes the turbocharger accelerate more quickly and allows the aggressive increase in the injection quantity to be started sooner, since the fuel quantity growth must follow the increase in the air supply in order to avoid high soot during transients.

55 Finally, after-injections can be applied to raise the diesel oxygen catalyst (*DOC*) temperature above its light-off
56 temperature after a cold start and post injections¹ can then be supplied to raise the exhaust temperature even further [15,
57 16].

58 Soot emissions are affected remarkably by the duration of the main injection. In fact, an important source of smoke
59 emissions exists in diesel engines at the end of main combustion, because both the equivalence ratio and local in-
60 cylinder temperature are high [17]. In particular, when long main-injection durations are considered, even a small
61 reduction in the energizing time of the main injection can provide significant soot benefits [18]. The shortened temporal
62 length of the main injection in multiple injection schedules featuring an after shot, produces less soot. Furthermore, the
63 contribution of soot from after-injected fuel, if planned correctly, can be lower than in the case in which the after-
64 injected fuel is included in the main injection [19]. When after-injection fuel is introduced into the combustion chamber,
65 the local equivalence ratio is lower than it is at the end of the main injection without after-injection. In fact, the fuel is
66 not injected at the same location since the piston is moving [20]. An enhanced air-fuel mixing occurs, due to the
67 presence of two separate smaller combustion events [10], according to a split flame type behaviour [17]. Furthermore,
68 improved particulate oxidation occurs later on in the combustion cycle, because of the increased in-cylinder bulk
69 temperatures during the expansion stroke [21].

70 An optimum main-after *DT* value, which depends on the after injected mass, exists for the optimization of the
71 interaction between the combustion of the main injection and the combustion of the after injection, as well as for the
72 subsequent minimization of the soot produced in the overall combustion [22]. In fact, if the *DT* is too short, the after
73 fuel is injected into the regions where the combustion of the main fuel takes place. The atomized fuel spray lacks
74 oxygen because the after-injection entrains the burned gases. As a result, combustion progresses gradually, causing a
75 low heat release peak and the slow combustion rate during diffusion combustion causes the smoke emissions to
76 increase. In these cases, the after-injection produces additional soot rather than oxidizing the previously formed soot, as
77 a consequence of the main injection. On the other hand, if the after pulse is too late, the combustion of the after fuel
78 occurs at excessively reduced temperatures and, although the soot production, which is due to the after injected fuel is
79 limited (this production becomes virtually null for an after injection into surrounding gases with lower temperatures
80 than 700 K [23]), the after-shot is once again unable to properly oxidize the soot produced during the main combustion.
81 The greatest smoke reduction is achieved when the start of the after-injection is phased within a tiny window of the
82 main diffusive flame [20] in order to guide the after-fuel into the squish volume [24]. The optimum *DT* value is in the
83 600÷1000 μ s range for passenger cars (instead the optimum after injection timing is in the 30-40° *CA ATDC* for delayed
84 main injection timings in heavy duty engines [25, 24]) and a constant *DT*, which corresponds to the optimum value, is
85 usually applied in the *ECU* maps for a medium speed and load range. As the mass of the after-injected fuel increases,

the main-after DT that minimizes the soot emissions, tends to augment. The quantity of the after injection is also a trade-off: if this quantity is too small, there is no significant effect of the after-shot and, if the fuel quantity is too high, the higher fuel mass has to burn in a high equivalence ratio environment [20]. The optimum after injection quantity is in the $1.5\div 3\text{ mm}^3$ range (around 15-20% of the total fuel mass in heavy duty engines [24]), i.e. small enough to prevent a quasi-steady diffusion flame from being established [23].

Main-after injection strategies also affect NO_x , $bsfc$ and CO engine-out emissions. The presence of an after injection can make the last part of the HRR curve of a pilot-main combustion rise faster than in the case without an after-injection, even though all the fuel is introduced earlier in the latter case [17]. The smaller the size of the after injection, the higher the acceleration of the final stage of combustion. Therefore, if a small after-injection is placed close to the main injection, the combustion process can conclude earlier than in the without the after-shot case. This can explain why the engine efficiency can be higher and the engine exhaust temperature can be lower when an early after-injection is used [26]. If the after-injection is phased close to the main injection, the combustion barycentre moves toward the TDC and the flame temperatures rise, thus leading to higher level of NO_x emissions and lower CO emissions than in the absence of the after shot. If the after-injection timing occurs sufficiently far from the main injection, the NO_x emissions improve compared to the without the after-injection case, whereas the fuel economy undergoes penalties for larger after injections, which lead to higher $bsfc$ reductions. Finally, the after-injection spray, for after injection timings at about $40^\circ CA ATDC$, reaches the wall of the liner, creating wall-wetting and thus rapidly increasing HC and $bsfc$ [27].

When heavy EGR rates (EGR fractions around 60%) are applied to control NO_x , most of the after injection cases generate an increment in the soot and in HC and CO , because the after injected fuel cannot burn well due to the poor oxygen concentration and delayed ignition [28]. This effect is in contrast with the main effect of after injection under moderate EGR rates (EGR fractions in the $25\div 40$ range). However, a small amount of fuel, injected in an after-injection with a short dwell time with respect to the main injection, can reduce fuel consumption, soot, HC and CO , compared to single injections, even for heavy EGR rates [29].

An after-injection can be effectively combined with one or more pilot shots in order to develop sophisticated injection strategies for the control of engine-out emissions, combustion noise and fuel consumption, in the medium load and speed area of a low-compression ratio engine. Contributions on this topic are available in the literature [27, 30, 31], but lack of information is still present about the impact of optimized calibrations featuring the after injection.

In the present work, the potentialities of triple and quadruple injection schedules are evaluated and the results on emissions and performance, in the presence of an after-shot, are compared with those referring to pilot-main and pilot-pilot-main injection strategies, at different steady-state engine working conditions. All the triple and quadruple injection engine calibrations have been optimized with the design of experiment (DoE) technique, and the pilot-main injection

117 engine calibration represented a state-of-the-art double injection calibration. This comparison between optimum
118 calibrations therefore allows the effective benefits of the after injection to be assessed. Furthermore, the after injection
119 is implemented in the presence of high *EGR* rates, whereas most of the researches on the after shot are conducted under
120 low or moderate *EGR* conditions [32].

121 3. EXPERIMENTAL SETUP AND ADOPTED INJECTION STRATEGIES.

122 The experimental tests have been carried out on the highly-dynamic test bench, installed at the Politecnico di Torino
123 ICEAL (IC Engines Advanced Laboratory) and equipped with an ‘ELIN AVL APA 100’ cradle-mounted AC
124 dynamometer. An ‘AVL KMA 4000’ has been used to continuously meter fuel consumption, with a reading accuracy of
125 0.1% over a 0.28-110 kg/h range. Furthermore, an ‘AVL AMAi60’ system, made up of different analyzer trains, has
126 been applied to measure the engine-out gaseous raw emissions of *HC*, *NO_x* and *CO*, as well as the *CO₂* levels in the
127 intake manifold, in order to evaluate the *EGR* rate. Finally, an AVL 415S smokemeter allows the engine-out soot
128 emissions to be evaluated in the exhaust gases.

129 The experimental data have been analyzed with the support of a previously developed three-zone combustion model
130 [33]. Ordinary differential mass and energy conservation equations have been applied to the fuel, unburned gas and
131 burned gas zones and have been solved numerically, on the basis of the experimental in-cylinder pressure. The model
132 allows the temperatures of the three zones to be predicted as functions of the crank angle. Furthermore, thermal and
133 prompt *NO* mechanisms are implemented in the code, according to the Zeldovich and Fenimore submodels,
134 respectively. The soot formation is modeled [42] by means of an expression that considers the mean air-fuel ratio over
135 the combustion period, while the soot oxidation rate is modeled using an empirical law, based on the temperature of the
136 burned gas zone.

137 Table 1 reports the scheme and the main features of the investigated Euro 5 passenger car diesel engine, fueled with
138 conventional diesel oil. This engine has been equipped with a *DOC* and a diesel particulate filter, while no
139 aftertreatment device has been designed to reduce the *NO_x* emissions. The engine has been fully instrumented with
140 piezoresistive pressure transducers and thermocouples, in order to measure the pressure and temperature in the intake,
141 exhaust and *EGR* lines of the engine. A high-frequency piezoelectric transducer has been installed in the glow-plug seat
142 to measure the pressure time-histories of the gases in the combustion chamber of one cylinder. Another piezoresistive
143 transducer has been used to detect the pressure levels in the inlet runner of the same cylinder and thus to reference the
144 in-cylinder pressure.

145 The implemented triple (both pilot-pilot-main and pilot-main-after) and quadruple (pilot-pilot-main-after) engine
146 calibrations have been optimized by means of the design of the experiments (*DoE*) statistical technique [8]. The

147 following parameters were considered as the most relevant input variables for the procedure: rail pressure (p_{Rail}), swirl
 148 actuator position (Sw), dwell times between consecutive injections (DT_{Pill} between the pilot 1 and main shots, DT_{Aft}
 149 between the main and after shots and DT_{Pil2} between the pilot 2 and pilot 1 shots in quadruple injection strategies, where
 150 pilot 1 is the closest shot to the main injection and pilot 2 the furthest shot from the main injection), main injection
 151 timing (SOI_{Main}), the injection quantities in each pilot or after shot (q_{Pill} , q_{Aft} and q_{Pil2} in quadruple injection strategies),
 152 the inducted air per stroke and per cylinder (m_a) and the boost pressure (p_{Boost}) at high load.

153 An engine working-point, evaluated as representative of engine application to a passenger car over the new European
 154 driving cycle, has been considered a key point. The following key-points were selected for the considered engine (n
 155 [rpm]× $bmeP$ [bar]): 1500×2, 1500×5, 2000×2, 2000×5, 2500×8, 2750×12 and idle.

156 For instance, Tables 2-4 report (second column) the parameter levels that were considered in the variation lists for the
 157 optimizations of the pMa injection schedule, at the 2000×5 and 2750×12 key-points, and of the $ppMa$ strategy, at the
 158 1500x5 key-point. The center and the extreme values of the levels that were considered for each parameter were chosen
 159 on the basis of preliminary measurements. An appropriate number of levels was selected in order to obtain accurate
 160 results with a reasonable number of tests for each variation list. The quantity of fuel in the main injection is set by the
 161 test-bench control system, in order to guarantee the $bmeP$ value, and is therefore not present as a parameter in the
 162 variation list. The inducted air (m_a), measured by means of the air mass flowmeter, was considered in the variation lists,
 163 instead of the EGR ratio. The p_{Boost} pressure only appears in the variation list of 2750x12 since has a lower influence for
 164 the other key points, which Tables 2 and 4 refer to. Furthermore, the simultaneous control of p_{Boost} and EGR can
 165 constitute a problem in the presence of high X_{EGR} values, which occur at key points 2000x5 and 2750x12.

166 The preliminary variation list of each considered key-point was obtained using the Matlab Model-Based Calibration
 167 toolbox, setting a V-optimal type design of experiments, which minimizes the prediction error variance, and a full
 168 factorial series, as the candidate set, on the basis of the levels shown in Tables 2-4. The final variation lists were made
 169 up of 120-150 tests for each considered key point, including replications of the central point (defined by the center
 170 value of the levels for each parameter).

171 Once the variation list tests had been carried out, on the engine, it was possible to obtain quadratic models of the output
 172 variables as functions of the input variables and of their interactions. The engine-out specific NO_x , CO , HC and soot
 173 emissions, the $bsfc$ and the CN were considered as the output variables. Different targets can be introduced for the
 174 output variables in order to select the best set of values for the input variables at each key point, that is, the optimized
 175 engine calibration. In the present work, the optimization strategy for the triple and quadruple injection calibrations,
 176 based on the DoE , has been aimed at minimizing the NO_x emissions and at reducing the combustion noise, compared to
 177 the pilot-main injection baseline calibration, which was originally implemented in the ECU provided by the engine

178 OEM. In fact, the goal is to avoid the application of any aftertreatment device for the NO_x emissions. The presence of a
179 $bsfc$ - NO_x trade-off constituted a constrain to the simultaneous reduction in $bsfc$ and NO_x and a slight increase in $bsfc$ has therefore
180 been accepted

181 Tables 5-7 show the reference values of the output variables for the pilot-main injection strategy and the constraints
182 used for the optimization of the triple and quadruple injection strategies, which Tables 2-4 refer to. The optimized
183 values of the input variables, calculated by means of the DoE procedure, are reported in the third column of Tables 2-4.
184 EGR trade-offs have been performed in the neighborhood of the baseline calibration points for the double, triple and
185 quadruple injection strategies, in order to compare not only the baseline points of the different calibrations, but the
186 complete EGR curves. The considered engine calibrations are characterized by elevated EGR mass fractions (
187 $X_{EGR} = \dot{m}_{EGR} / (\dot{m}_a + \dot{m}_{EGR})$), within the 45-55% range.

188 4 PILOT-MAIN-AFTER INJECTION STRATEGIES.

189 If reference is made to the pilot-main (pM) and pilot-main-after (pMa) baseline calibrations at $bmeP=5$ bar and $n=2000$
190 rpm, the addition of an after injection, featuring a relatively late timing ($SOI_{after} \approx 20^\circ$ CA ATDC) with respect to the
191 main injection, leads to a significant reduction in the NO_x emissions (cf. Fig. 1, the contoured triangle and circle
192 symbols) and in CN (cf. Fig. 2, the contoured triangle and circle symbols), while $bsfc$, soot, HC, and CO (cf. Figs. 3-6,
193 the contoured triangle and circle symbols) become worse. However, the penalties on soot, HC and CO are acceptable,
194 since the engine is equipped with both a DOC and a particulate filter. In general, CN improves by about 1.2÷1.5 dB for
195 the different X_{EGR} values in the pMa case (Fig. 2), while the $bsfc$ - NO_x , soot- NO_x , HC- NO_x and CO- NO_x EGR trade-off
196 curves (Figs. 3-6) coincide for the pM and the pMa strategies.

197 Figures 7-10 compare the crankshaft angle based distributions of the HRR, T_b , NO_x and soot for the baseline calibrations
198 of the pM and the pMa strategies (as previously mentioned, the pMa baseline calibration is the output of the DoE
199 optimization procedure). Since the timing adopted for the after-injection is delayed, the after combustion (Fig. 7) takes
200 place under low in-cylinder pressure and gas temperatures (Fig. 8), and the peak burned gas temperature also reduces
201 for the pMa strategy, due to the higher X_{EGR} value. Furthermore, the residence time of the burned gases at higher
202 temperatures than 1950 K is longer for the pM calibration (Fig. 8). Finally, the proximity of the pilot combustion to the
203 main combustion and the increased X_{EGR} value can lead to richer stoichiometric equivalence ratios for the pMa strategy
204 at the start of the main combustion. All of these circumstances induce increased NO_x emissions for the pM strategy,
205 compared to the without after-injection case (Fig. 9), because the thermal NO_x increase with the value of the flame
206 temperature during the diffusive portion of combustion and are only produced in the presence of sufficient O_2
207 concentrations in the post-flame zones [34]. The reduced DT between the pilot and main injection in the pMa strategy

allows a softer transition between the pilot and main combustion (the *HRR* peak of the main combustion is higher for the *pM* case), and is therefore beneficial in suppressing combustion noise.

As far as the *PM* is concerned (Fig. 10), the low-temperature combustion of the after-injected fuel does not generally oxidize the previously formed soot. Furthermore, the presence of heavy *EGR* rates prevents the after-injected fuel from burning well, because of a lack of oxygen concentration. As a consequence, the after injection on its own produces increments in the quantity of the particulate matter, and this is proved by the change in rate, which occurs at $\theta \approx 385^\circ CA$ along the soot curve of the *pMa* strategy. The higher soot level obtained for the *pMa* strategy is also the result of the lower premixed portion of its main combustion: in fact, the *HRR* peak pertaining to the main combustion in Fig. 7 is higher for the *pM* strategy than for the *pMa* one.

As already mentioned, the *pMa* calibration selected in the present case has had the aim of reducing the NO_x emissions and combustion noise [35]; the soot emissions are controlled by the retarded SOI_{Main} ($\approx 2^\circ CA ATDC$) and, above all, by the diesel particulate filter (cf. also Table 5).

The *HC* and *CO* emissions in Figs. 5 and 6 are higher for the *pMa* baseline calibration point because of the retarded after combustion [36, 10], which causes incomplete oxidation, and because of the possible presence of a greater number of over-rich mixture zones at the start of combustion of the main injected fuel (cf. also Table 5).

Finally, the delayed after-injection (cf. *MFB50* values in Fig. 11) raises the temperature at the engine exhaust (cf. T_{exh} in Fig. 12) for the *pMa* baseline calibration. This leads to a larger thermal energy loss at the engine exhaust and thus explains the slight deterioration in the *bsfc*, shown in Fig. 3, and also found in [37]. On the other hand, the higher T_{exh} values can be exploited to reduce the turbocharger lag during engine transients.

Figures 13-20 refer to $n=2500$ rpm and $bmeP=8$ bar. The main difference in the *HRR* diagrams in Fig. 13, compared to those in Fig. 7, concerns the position of the pilot injection, which occurs earlier for the *pMa* strategy. Furthermore, the rail pressure level is $p_{rail} \approx 1200$ bar at this key-point for the *pM* calibration, whereas it reduces to $p_{rail} \approx 1125$ bar for the *pMa* calibration (a higher injection pressure promote a better air-fuel mixing [38]). No pilot combustion occurs in the *pMa* case, and the role of the main injection is therefore to trigger fuel ignition, which can cause interference between the pilot injected fuel flames and the main injection (the soot increases significantly in Fig. 17 for the *pMa* case).

The NO_x and *CN* are lower for the baseline point of the *pMa* calibration (cf. Fig. 20), and the causes of the improved NO_x are again the decreased residence time of the burned gas at very high temperatures, the reduced p_{nom} value and the relatively high local equivalence ratios in the $360^\circ CA < \theta < 390^\circ CA$ range (cf. Figs 14 and 15). The soot and *CO* emissions are better for the *pM* injection baseline calibration (cf. Figs. 17 and 19) and the reasons for this are the same as those provided for the previously analyzed engine key-point. However, unlike for $n=2000$ rpm and $bmeP=5$ bar, the soot- NO_x and *CO-NO_x* trade-offs become slightly worse for the *pMa* strategy, and the *CN-NO_x* curve of the *pMa*

strategy is no better than that of the *pM* strategy. The general improvement in the *HC* emissions that results from the application of the *pMa* injection schedule (cf. Fig. 18) is related more to the absence of the pilot combustion (the main injection triggers the ignition of the pilot injected fuel for the *pMa* strategy and this probably reduces the occurrence of overleaning) or to the reduced rail pressure level than to the addition of the after shot. The *bsfc-NO_x* trade-off, the soot-*NO_x* trade-off, the *CO-NO_x* trade-off and the *CN-NO_x* *EGR* curve for *n*=2750 rpm and *bme_p*=12 bar are reported in Figs. 21-24. The *pMa* calibration improves the soot-*NO_x* and the *CO-NO_x* trade-offs, but penalties are incurred in *bsfc* (cf. also Table 6). The *HC-NO_x* trade-off also improves for the *pMa*, but the *HC* values are lower than 0.1 g/kWh for both strategies and are therefore not a cause of concern. The *CO* emission levels in Fig. 23 are not critical either.

5 PILOT-PILOT-MAIN-AFTER INJECTION STRATEGIES.

Double *pM* and triple *ppM* injection strategies have been compared with *pMa* and *ppMa* strategies at medium load and speed conditions. Figures 25-29 report the experimental results at *bme_p*=5 bar and *n*=1500 rpm for the different calibrations. The triple injections (either *ppM* or *pMa*) do not improve the *bsfc-NO_x* (Fig. 25), soot-*NO_x* (Fig. 26) *HC-NO_x* (Fig. 27) or *CO-NO_x* (Fig. 28) *EGR* trade-offs, compared to the *pM* calibration. The *CN-NO_x* curve (cf. Fig. 29) does not change either when passing from the *pM* to the *ppM* or *pMa* injection schedules. No discrepancy can be observed between the results concerning *CN* in Fig. 29 and those reported in Figs. 2, which refer to a similar working condition. In fact, the higher the engine speed at fixed *bme_p*, the higher the combustion noise levels [39]. Furthermore, Fig. 30 shows that the pilot and main combustion events are clearly distinct for both the *pM* and the *pMa* baseline calibration points, unlike the events shown in Fig. 7, where the transition from the pilot to the main combustion was softer for the *pMa* strategy and this explained the lower *CN* (the difference between the main combustion *HRR* peaks of the *pM* and *pMa* calibrations is greater in Fig. 7 than in Fig. 30). Finally, the ignition delay of the main injected fuel in Fig. 30 is slightly longer, and the *HRR* peak attributed to the pilot combustion is higher for the *pMa* schedule than for the *pM* one; both these results are physically consistent with the *CN* increase detected for the *pMa* calibration [40]. In short, the after-injection only seems to have an indirect impact on the management of combustion noise. The addition of the after shot to an injection train can produce relevant changes in the optimized *DoE* calibration. In particular, the presence of the after injection can modify certain pilot injection parameters, such as pilot injection quantity and timing. These parameters can influence the interaction between the pilot mixture field and the main injection, that is, the way the main injection interferes with the ignition process of the pilot mixture and influences its combustion process, and

269 thus can significantly affect the combustion noise [40]. In general, in addition to the described interaction, hydraulic
 270 interference between the pilot and main injections may also occur [41]. In fact, the different sets of pilot injection
 271 masses and timings can generate different pressure values in the injector delivery chamber at the SOI_{main} instant, due to
 272 the variability in the pressure wave dynamics. Therefore, the velocity at which the needle opens the nozzle during the
 273 main energizing time can vary for the different calibrations and this can have an appreciable impact on the noise. In
 274 general, the higher the needle velocity at the beginning of the main injection, the higher the combustion noise. This
 275 hydraulic effect can be remarkable when pilot injections with lower DT than $500\ \mu s$ are implemented, [6], but it is not
 276 significant for the pilot-main DT considered in Fig. 30, (the enlargement in Fig. 30 shows smaller differences than 20%
 277 in the injected flow-rate slope).

278 The $ppMa$ calibration allows the $bsfc-NO_x$ and the $CN-NO_x$ EGR curves in Figs. 25 and 29 to be improved (cf. Table 7).
 279 A slight benefit can also be observed in the management of the soot- NO_x trade-off (cf. Fig. 26). On the other hand, no
 280 benefits can be observed for the quadruple injection with respect to the $HC-NO$ (Fig. 27) or to the $CO-NO_x$ (Fig. 28)
 281 EGR trade-offs, compared to pM and ppM strategies.

282 Figures 31-33 report the burned gas temperature, the NO_x and the soot in-cylinder angular distributions for the baseline
 283 calibration points of the four considered injection strategies. These diagrams, together with the HRR traces, complete
 284 the in-cylinder numerical analysis. Even though $ppMa$ features the highest T_b values (Fig. 31), the NO_x engine-out
 285 emissions are minimized (Fig. 32). This behavior is probably due to the equivalence ratio distributions within the
 286 cylinder.

287 Part of the fuel injected in the later-pilot injection burns during the main injection event in the $ppMa$ baseline calibration
 288 (cf. Fig. 30), and a larger amount of rich mixture (with $\phi \geq 2$) results in the fuel spray of the main injection (the global O_2
 289 concentration is also minimum for the $ppMa$ case). As a consequence, the NO_x emissions diminish. For the same reason,
 290 a great peak of soot can be seen in Fig. 33 for the $ppMa$ case, although the energizing time of the main injection is
 291 reduced, and the high T_b values and the appropriate timing of the after-injection, with respect to the main shot ($DT \approx 600$
 292 μs), promote a greater oxidation of the soot generated during the main combustion. The pM baseline calibration shows
 293 lower interference between pilot combustion and the main injection and employs the lowest X_{EGR} value. As a result, a
 294 soot level minimum can be found at the engine exhaust (cf. Fig. 33). On the other hand, the high T_b values encountered
 295 during diffusive combustion could explain the great increase in the NO_x over the $370^\circ CA < \theta < 390^\circ CA$ range for this
 296 strategy. Furthermore, a significant production of NO_x also occurs for the pM strategy during the diffusive portion of
 297 pilot-injected-fuel combustion, i.e., over the $360^\circ CA < \theta < 365^\circ CA$ range.

298 In the case of the *ppM* calibration, the higher rail pressure nominal value, i.e. $p_{rail} \approx 750$ bar instead of $p_{nom} \approx 620$ bar,
299 which is applied to all the other strategies at 1500x5, is responsible for the relatively high NO_x engine-out emissions that
300 can be observed in Fig. 32.

301 As far as the pilot injection is concerned, the highest temperatures of the unburned gases (cf. Fig. 31 for $\theta < 350^\circ CA$),
302 the reduced ignition delay of the fuel injected in the earlier pilot shot, and the major interference between the
303 combustion event pertaining to the earlier pilot injection and the fuel injected in the later pilot shot, are the reasons for
304 the augmented soot production over the $350^\circ CA < \theta < 365^\circ CA$ interval in the *ppMa* case (cf. also Table 7).

305 The less steep pattern of the *HRR* curve for the *ppMa* calibration is the reason for the general lower combustion noise
306 level in Fig. 29. This *HRR* pattern is induced by the reduced entity of the premixed combustion, as a consequence of the
307 more pronounced interaction between the oxidation of the fuel, which is injected in the later pilot injection shot, and the
308 main injection.

309 6 CONCLUSIONS.

310 Multiple injection strategies featuring an after shot have been compared with pilot-main and pilot-pilot-main injection
311 strategies in a low-compression ratio Euro 5 diesel engine, in order to evaluate the possible benefits in engine-out
312 emissions, combustion noise and fuel consumption, at medium to high loads and at low to medium speeds.

313 All the triple and the quadruple injection strategies considered in this work have been optimized by means of a *DoE*
314 procedure: this aspect is relevant because it allows the effective benefits of the after injection to be assessed. *EGR* trade-
315 offs have been carried out around the baseline calibration points obtained from the *DoE* and around the *pM* injection
316 calibration. The latter represented the state-of-the-art double injection calibration of the considered engine technology.
317 Experimental tests have been conducted in a dynamometer cell and different steady-state key-points, which were
318 representative of the medium-high part load zone of the *NEDC* for a passenger car engine application, have been
319 considered. The experimental analysis has been supported by numerical results, which were derived from the
320 application of diagnostic combustion models, on the basis of the measured trace of the in-cylinder pressure time history.
321 The main outcomes concerning the effects of the after injection on pilot-main injection strategies with postponed main
322 injection timings are reported synthetically hereafter.

323 • At medium to high loads and medium speeds, *DoE* optimized calibrations featuring after-injections with delayed
324 timings ($10\text{-}15^\circ CA ATDC$) can improve engine-out NO_x emissions, compared to the *pM* baseline calibration, because
325 the after-injections take place at low in-cylinder pressures and gas temperatures. However, since the applied DT_{Aft}
326 values are relatively large, soot emissions grow and *bsfc* is slightly higher than in the case of the *pM* baseline

327 calibration. Furthermore, *CO* engine-out emissions tend to become worse for the *pMa* baseline calibration, due to the
328 reduced temperatures of the after combustion.

329 • The soot-*NO_x*, *bsfc-NO_x* and *CO-NO_x* trade-offs of the engine calibration that employs the after injection do not
330 change significantly, compared to those referring to a *PCCI* late strategy featuring a pilot-main injection schedule.
331 Furthermore, the addition of the after-injections does not show any clear effect on the *HC-NO_x* trade-off, which can
332 either improve or become worse, depending on the considered *bme_p* and *n* values. However, the *HC* engine-out
333 emissions are not a concern at medium speed and medium to high loads, which represent the typical working conditions
334 of the after injection strategy.

335 • After-injection only seems to have only an indirect impact in the management of combustion noise. The addition of
336 the after-shot to an injection train can produce relevant changes in a *DoE* optimized calibration. In particular, the
337 presence of an after-injection can modify certain pilot injection parameters, such as the pilot injection quantities and
338 timings. These parameters can influence the interaction between the pilot mixture field and the main injection, i.e., the
339 way the main injection interferes with the ignition process of the pilot mixture and influences its combustion process.
340 All this can have a significant effect on combustion noise. As proof of the complex correlation between the after-shot
341 and combustion noise, a comparison between the *pM* and *pMa* experimental data has shown that, for the *pMa*
342 calibration, the *CN* generally improves by 2 dB at *bme_p*=5 bar and *n*=2000 rpm, but generally deteriorates by 1 dB at
343 *bme_p*=5 bar, *n*=1500 rpm and at *bme_p*=12 bar, *n*=2750 rpm.

344 • The application of *ppMa* injection schedules at medium load and speed leads to improvements in the soot-*NO_x*,
345 *bsfc-NO_x* trade-offs, compared to the *pM* and *ppM* strategies. Furthermore, *CN* reduces significantly, while the *CO-NO_x*
346 trade-offs do not become worse. The presence of four injection shots leads to an increased flexibility in the management
347 of the different constraints and in particular in the design of the best interaction between the pilot injection combustions
348 and the main injection. A combination of *ppMa* strategies and high *EGR* rates is therefore recommended in low-
349 compression ratio engines featuring delayed main injection timing.

350 7 NOMENCLATURE.

351	<i>bme_p</i>	brake mean effective pressure
352	<i>bsfc</i>	brake specific fuel consumption
353	<i>CA</i>	crankshaft angle degree
354	<i>CN</i>	combustion noise
355	<i>DOC</i>	diesel oxygen catalyst
356	<i>DoE</i>	design of experiments

357	DT	dwel time
358	ECU	electronic control unit
359	EGR	exhaust gas recirculation
360	HC	unburned hydrocarbons
361	HRR	heat release rate
362	m_a	fresh air mass per stroke and per cylinder
363	\dot{m}_a	fresh air mass flow-rate
364	\dot{m}_{EGR}	exhaust gas recirculation mass flow-rate
365	$MFB50$	angle at which 50% of the combustion mixture has burned
366	n	engine speed
367	NO_x	nitrogen oxides
368	$O_{2\ int}$	oxygen volume concentration
369	p_{Boost}	boost pressure
370	p_{int}	pressure in the intake manifold
371	p_{cyl}	in-cylinder pressure
372	p_{rail}	nominal rail pressure level
373	$PCCI$	premixed charge compression ignition
374	PM	particulate matter
375	q	injected quantity (volume)
376	TDC	top dead center
377	SOI	electrical start of the injection
378	Sw	swirl actuator position
379	T_b	burned gas temperature
380	TDC	top dead center
381	X_{EGR}	mass fraction of exhaust gas recirculation
382	ϕ	equivalence ratio
383	λ	relative air-to-fuel ratio
384	θ	crankshaft angle in the simulations
385	<u>Subscripts</u>	
386	$Main$	main injection

387 *Pil1* pilot 1 injection
 388 *Pil2* pilot 2 injection
 389 *Aft* after injection

390 **8 REFERENCES.**

- 391 [1] Mohan, B., Yang, W., and Chou, S. K., 2013, "Fuel injection strategies for performance improvement
 392 and emissions reduction in compression ignition engines — A review", *Renewable and Sustainable Energy*
 393 *Reviews*, vol. 28, pp. 664-676.
- 394 [2] Fang, Q., Fang, J., Zhuang, J., and Huang, Z., 2012, "Influences of pilot injection and exhaust gas
 395 recirculation (*EGR*) on combustion and emissions in a HCCI-DI combustion engine", *Applied Thermal*
 396 *Engineering*, vol. 48, pp. 97-104.
- 397 [3] Suh H.K., 2011, "Investigations of multiple injection strategies for the improvement of combustion and
 398 exhaust emissions characteristics in a low compression ratio (CR) engine", *Applied Energy* 88 pp. 5013–
 399 5019. doi:10.1016/j.apenergy.2011.06.048.
- 400 [4] Zheng M., Kumar R., 2009, "Implementation of multiple-pulse injection strategies to enhance the
 401 homogeneity for simultaneous low-NO_x and -soot diesel combustion". *International Journal of Thermal*
 402 *Sciences* 48 pp. 1829–1841. doi:10.1016/j.ijthermalsci.2009.02.009.
- 403 [5] Kremer, F., Schaub, J., Steffens, C., and Kolbech, A., 2012 "Optimizing the noise of future passenger car
 404 diesel engines", *MTZ*, vol. 74, pp. 50-55.
- 405 [6] Ferrari, A., Mittica, A., and Spessa, E., 2013, "Benefits of hydraulic layout over driving system in piezo-
 406 injectors and proposal of a new-concept CR injector with an integrated Minirail", *Apply Energy*, vol. 103, pp.
 407 243-255.
- 408 [7] Ferrari, A., Paolicelli, F., and Pizzo, P., 2015, "The new-generation of solenoid injectors equipped with
 409 pressure-balanced pilot valves for energy saving and dynamic response improvement"; *Applied Energy*, 151,
 410 pp. 367-376.

- 411 [8] d'Ambrosio, S., and Ferrari, A., 2014, "Potential of double pilot injection strategies optimized with a
412 design of experiments procedure in the improvement of diesel engine emissions and performance",
413 submitted to *Applied Energy*.
- 414 [9] Helmantel, J., Somhorst, J., and Denbratt, I., 2003, "Visualization of the effects of post injection and
415 swirl on the combustion process of a passenger car Common Rail DI diesel engine", ICES2003-622,
416 Proceedings of the ASME conference, Salzburg.
- 417 [10] Chen, S. K., 2000, "Simultaneous reduction of NO_x and particulate emissions by using multiple
418 injections in a small engine", SAE Paper No.° 2000-01-3084.
- 419 [11] Surushima, T., Zhang, L., and Ishii, Y., 1999, "A study of unburned HC emission in small DI diesel
420 engines", SAE Paper No. 1999-01-0512.
- 421 [12] Dronniou, N., Lejeune, M., Balloul, I., and Higelin, P., 2005, "Combination of High EGR Rates and
422 Multiple Injection Strategies to Reduce Pollutant Emissions," SAE Paper No. 2005-01-3726, 2005.
- 423 [13] Zheng, Z., Lang, Y., Liu, H., Zhu, Y., Zhong, X., and Yao, M., 2015, "Effect of two-stage injection on
424 combustion and emissions under high EGR rate on a diesel engine by fueling blends of diesel/gasoline,
425 diesel/n-butanol, diesel/gasoline/n-butanol and pure diesel", *Energy Conversion and Management*, vol. 90,
426 pp. 1-11.
- 427 [14] Walker, L.C., et al., 2011, "Method and system for reducing turbo lag in an engine", US Patent
428 Application 11/464.888 (Navistar).
- 429 [15] Parks, J., Huff, S., Kass, M., Sorey, J., 2007, "Characterization of in-cylinder techniques for thermal
430 management of diesel aftertreatment", SAE Paper No. 2007-01-3997.
- 431 [16] Guo, G., Warner, J., Cavataio, G., Dobson, D., Badillo, E., and Lambert, C., 2010, "The development of
432 advanced urea-SCR systems for Tier 2 Bin 5 and beyond diesel vehicles", SAE Paper No. 2010-01-1183.
- 433 [17] Desantes, J. M., Arrègle, J., Lopez, J. J., and Garcia, A., 2007, "A comprehensive study of diesel
434 combustion and emissions with post injection", SAE Paper No. 2007-01-0915.

- 435 [18] Dieselnets website, since 1997, "Engine & emission technology online", www.dieselnets.com.
- 436 [19] Han, Z., Uludogan, A., Hampson, G. J., Reitz, R. D., 1996, "Mechanism of soot and NO_x emission
437 reduction using multiple injection in a diesel engine", SAE Paper No. 960633.
- 438 [20] Mendez, S., and Thirouard, S., 2008, "Using Multiple Injection Strategies in Diesel Combustion:
439 Potential to Improve Emissions, Noise and Fuel Economy Trade-off in Low CR engines", *SAE Int. J. Fuels
440 Lubr.*, Vol. 1, Issue 1, pp. 662-674.
- 441 [21] Yun, H. H., Sellnau, M., Milovanovic, N., and Zuelch, S., 2008, "Development of premixed low-
442 temperature diesel combustion in a HSDI engine", SAE Paper No. 2008-01-0639.
- 443 [22] Park, C., Kook, S., and Bae, C., 2004, "Effects of multiple injections in a HSDI diesel engine equipped
444 with Common Rail injection system", SAE Paper No. 2004-01-0127.
- 445 [23] Arregle, J., Pastor, J. V., Lopez, J. J., and Garcia, A., 2008, "Insights on post injection-associated soot
446 emissions in direct injection strategies", *Combustion and Flame*, 154, pp. 448-461.
- 447 [24] Bobba, M., and Musculus, M., 2010 "Effects of post injections on in-cylinder and exhaust soot for low-
448 temperature combustion in a heavy-duty diesel engine", *SAE Int. J. Engines*, Vol. 3, issue 1, p. 497.
- 449 [25] Ojeda, W.D., Zoldak, P., Espinosa, R., and Kumar, R., 2009, "Development of a Fuel Injection Strategy
450 for Partially Premixed Compression Ignition Combustion," *SAE Int. J. Engines* 2(1):1473-1488.
- 451 [26] Thurnheer T., Edenhauser D., Soltic P., Schreiber D., Kirchen P., and Sankowski A., 2011,
452 "Experimental investigation on different injection strategies in a heavy-duty diesel engine: Emissions and
453 loss analysis", *Energy Conversion and Management*, 52, pp. 457-467.
- 454 [27] Lee, J. W., Choi, H., Hong, K., Lee, S., Yu, S., Choi, S.M., and Min, K.D., 2013, "Comparison of the
455 effects of multiple injection strategy on the emissions between moderate and heavy EGR rate conditions: part
456 2-post injections", *Journal of Mechanical Science and Technology*, 27(7), pp. 2217-2223.
- 457 [28] Helmantel, A., and Golovitchev, 2009, "Injection strategy optimization for a light duty DI diesel engine
458 in medium load conditions with high EGR rates", SAE Paper No. 2009-01-1441.

- 459 [29] Lee, J. W., Choi, H., Lee, S., Shin, S., Choi, S. M., Song, H., and Min, K. D., 2012, "Emission reduction
460 by close post injection strategy with modified nozzle and piston bowl geometry at diesel combustion with
461 heavy *EGR* rate", SAE Paper No. 2012-01-0681.
- 462 [30] Badami, M., Mallamo, F, and Millo, F., 2003, "Experimental investigation on the effect of multiple
463 injection strategies on emissions, noise and brake specific fuel consumption of an automotive direct injection
464 common-rail diesel engine", *International journal of engine research* 4(4), pp. 299-314.
- 465 [31] Badami, M., Mallamo, F, and Millo, F., 2002, "Analysis of multiple injection strategies for the
466 reduction of emissions, noise and bsfc of DI CR small displacement non-road diesel engine", SAE Paper
467 No. 2002-01-2672.
- 468 [32] Zheng Z., Yue L., Liu H., Zhu Y., Zhong X., and Yao M., 2015, "Effect of two-stage injection on
469 combustion and emissions under high *EGR* rate on a diesel engine by fueling blends of diesel/gasoline,
470 diesel/n-butanol, diesel/gasoline/n-butanol and pure diesel", *Energy Conversion and Management*, 90, pp. 1-
471 15.
- 472 [33] Finesso, R., and Spessa, E, 2014, "A real time zero-dimensional diagnostic model for the calculation of
473 in-cylinder temperatures, HRR and nitrogen oxides in diesel engines. *Energy Conversion and Management*
474 79 498–510. <http://dx.doi.org/10.1016/j.enconman.2013.12.045>.
- 475 [34] Akihama, K., Takatori, Y., Inagaki, K., Sakaki, S., and Dean, A. M., 2001, "Mechanism of smokeless
476 rich diesel combustion by reducing temperature", SAE Paper No. 2001-01-0655.
- 477 [35] Mohan, B., Yang, W., and Chlu, S. K., 2013, "Fuel injection strategies for performance improvement
478 and emission reduction in compression ignition engines - A review", *Renewable and Sustainable Energy*
479 *Reviews*, 28, pp. 664-676.
- 480 [36] Lee, J. W., Choi, S. M., Shin, S. H., Choi, M., and Min, K. D., 2012, "Experimental analysis of
481 emission reduction by the split injection strategy using close post injection with a double-row nozzle in
482 heavy *EGR* conditions", *Journal of Mechanical Science and Technology*, 26(4), pp. 1-10.

- 483 [37] Zhuang J, Qiao X, Bai J, Hu Z, 2014, "Effect of injection-strategy on combustion, performance and
484 emission characteristics in a DI-diesel engine fueled with diesel from direct coal liquefaction", *Fuel* 121 pp.
485 141–148. <http://dx.doi.org/10.1016/j.fuel.2013.12.032>.
- 486 [38] Gan S, Ng HK, Pang KM, 2011, "Homogeneous charge compression ignition (HCCI) combustion:
487 implementation and effects on pollutants in direct injection diesel engines". *Applied Energy*;88(3):559–567.
- 488 [39] Priede, T., 1979, "Problems and Developments in Automotive Engine Noise Research," SAE Technical
489 Paper No. 790205.
- 490 [40] Busch, S., Zha, K., and Miles, P. C., 2014, "Investigations of closely coupled pilot and main injections
491 as a mean to reduce combustion noise", Thiesel Conference, September 9th-12th, Valencia, Spain.
- 492 [41] Herfatmanesh M.R., Lu P., Attar M.A., and Zhao H., 2013, "Experimental investigation into the effects
493 of two-stage injection on fuel injection quantity, combustion and emissions in a high-speed optical common
494 rail diesel engine", *Fuel* 109 pp. 137–147. <http://dx.doi.org/10.1016/j.fuel.2013.01.013>.
- 495 [42] Baratta M., Catania A.E., Ferrari A., Finesso R. and Spessa E., 2011, "Premixed-Diffusive Multizone
496 Model for Combustion Diagnostics in Conventional and PCCI Diesel Engines", *ASME Trans. Journal of*
497 *Engineering for Gas Turbines and Power*, vol. 133 n. 10, Art. No. 102801, pp. 1-13.

Engine type	2.0L Euro 5
Displacement	1956 cm ³
Bore × stroke	83.0 mm × 90.4 mm
Compression ratio	16.3
Valves per cylinder	4
Turbocharger	Twin-stage with valve actuators and WG
Fuel injection system	CR 2000 bar piezoelectric indirect acting injectors
Specific power and torque	71 kW/l – 205 Nm/l
EGR system type	Short-route cooled EGR

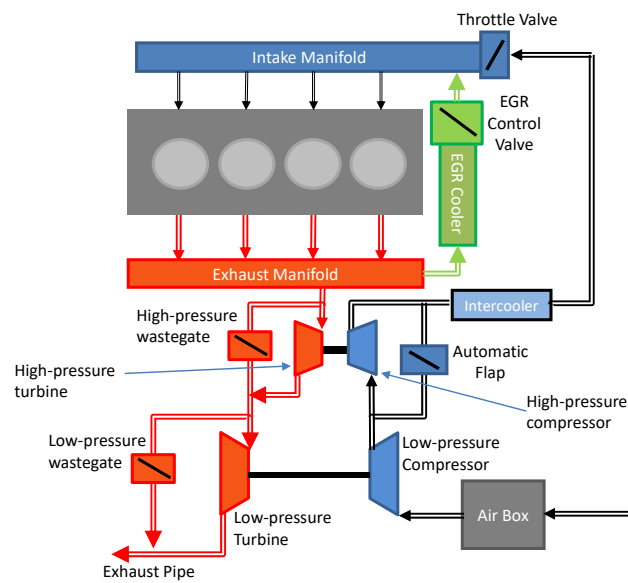


Table 1: Main specifications of the reference engine.

Quantity	Levels	Optimization
SOI_{Main} [°CA bTDC]	-3 -1 1	1
m_a [mm ³ /(stk·cyl)]	360 380 390 400 420	384
S_w [%]	30 40 50	30
p_{Rail} [bar]	750 850 950 1050 1150	750
q_{Pil} [mm ³ /(stk·cyl)]	0.8 1.1 1.4 1.7 2	1.42
DT_{Pil} [μs]	600 850 1100 1350 1600	600
q_{Aft} [mm ³ /(stk·cyl)]	1 1.5 2 2.5 3	1
DT_{Aft} [μs]	600 933 1267 1600 1933 2267 2600	1082

Table 2: Levels considered for the variation list and optimized values of the inputs for the pMa injection strategy at 2000×5.

Quantity	Levels	Optimization
SOI_{Main} [°CA bTDC]	4 5 6 7 8	6.19
m_a [mm ³ /(stk·cyl)]	680 690 700 710 720	720
Sw [%]	10 27.5 45	25
p_{Rail} [bar]	1500 1575 1650 1725 1800	1504.3
q_{Pil} [mm ³ /(stk·cyl)]	0.7 1 1.3	0.7
DT_{Pil} [μs]	800 1000 1200 1400 1600	1600
q_{Aft} [mm ³ /(stk·cyl)]	0.7 1.25 1.8 2.35 2.9 3.45 4	0.7
DT_{Aft} [μs]	800 950 1100 1250 1400	1203
p_{Boost} [mbar]	2200 2300 2400 2500 2600	2563

Table 3: Levels considered for the variation list and optimized values of the inputs for the pMa injection strategy at 2750×12.

Quantity	Levels	Optimal
SOI_{Main} [°CA bTDC]	-4 -2 0	0
m_a [mm ³ /(stk·cyl)]	340 357.5 392.5 410	358.1
S_w [%]	30 40 50	44
p_{Rail} [bar]	600 700 800 900 1000	620.1
q_{Pill} [mm ³ /(stk·cyl)]	0.8 1.1 1.4 1.7 2	1
DT_{Pill} [μs]	600 850 1100 1350 1600	905
q_{Pill2} [mm ³ /(stk·cyl)]	0.8 1.15 1.5	0.8
DT_{Pill2} [μs]	600 850 1100 1350 1600	614
q_{Aft} [mm ³ /(stk·cyl)]	0.8 1.35 1.9 2.45 3	0.8
DT_{Aft} [μs]	600 1000 1400 1800 2200 2600 3300	684

Table 4: Levels considered for the variation list and optimized values of the inputs for the ppMa injection strategy at 1500×5.

Strategy	NO _x [g/kWh]	HC [g/kWh]	CO [g/kWh]	Soot [g/kWh]	bsfc [g/kWh]	CN [dBA]
pM	0.99	0.3	1.9	0.3	247	86.5
pMa	min	≤0.5	≤3	≤0.7	≤250	≤86.5

Table 5: Reference values of the reference *pM* calibration baseline point and constraints for the optimization of the *pMa* injection strategy at 2000×5.

Strategy	NO _x [g/kWh]	HC [g/kWh]	CO [g/kWh]	Soot [g/kWh]	bsfc [g/kWh]	CN [dBA]
pM	1.7	0.09	0.9	0.17	223	87.1
pMa	min	≤0.1	≤0.9	≤0.3	≤230	≤87.1

Table 6: Reference values of the reference pM calibration baseline point and constraints for the optimization of the *pMa* injection strategy at 2750×12.

Strategy	NO _x [g/kWh]	HC [g/kWh]	CO [g/kWh]	Soot [g/kWh]	bsfc [g/kWh]	CN [dBA]
pM	0.89	0.33	1.8	0.17	235	80.5
ppMa	min	≤0.33	≤2	≤0.4	≤235	≤79

Table 7: Reference values of the reference *pM* calibration baseline point and constraints for the optimization of the *ppMa* injection strategy at 1500×5.

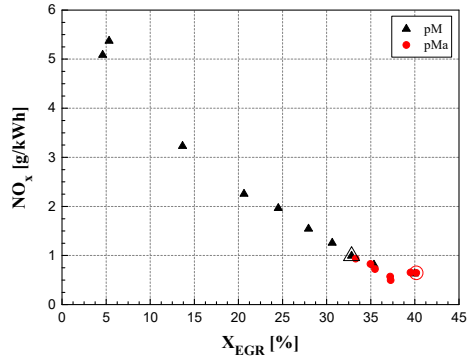


Figure 1. NO_x - X_{EGR} curve for the *pM* and *pMa* strategies ($b_{mep}=5$ bar, $n=2000$ rpm).

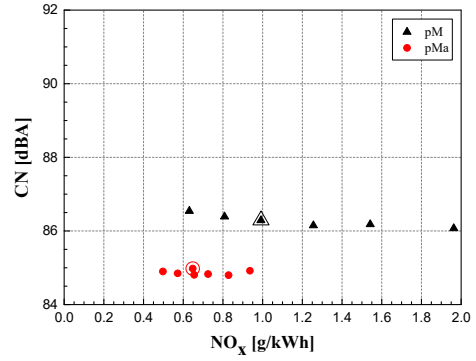


Figure 2. CN - NO_x trade-off for the *pM* and *pMa* strategies ($b_{mep}=5$ bar, $n=2000$ rpm).

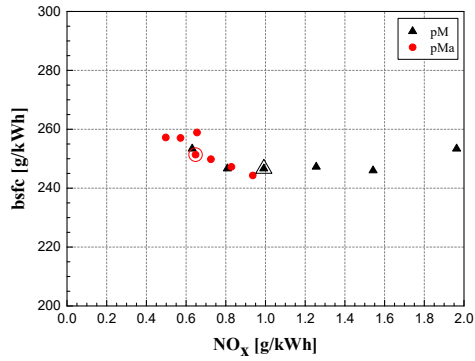


Figure 3. $bsfc$ - NO_x trade-off for the *pM* and *pMa* strategies ($b_{mep}=5$ bar, $n=2000$ rpm).

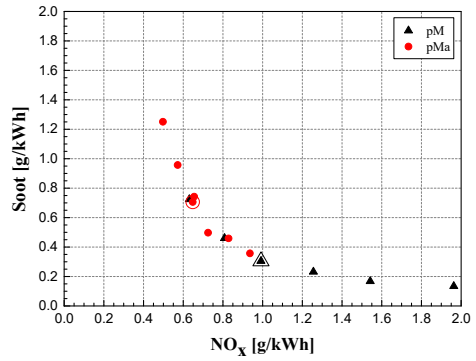


Figure 4. CO - NO_x trade-off for the *pM* and *pMa* strategies ($b_{mep}=5$ bar, $n=2000$ rpm).

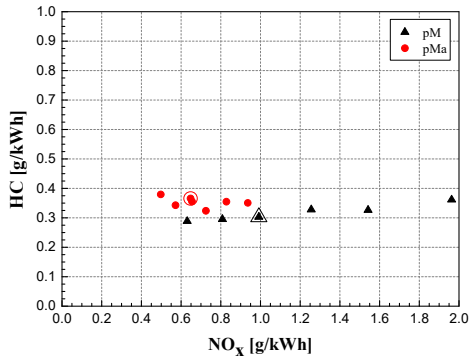


Figure 5. HC - NO_x trade-off for the *pM* and *pMa* strategies ($b_{mep}=5$ bar, $n=2000$ rpm).

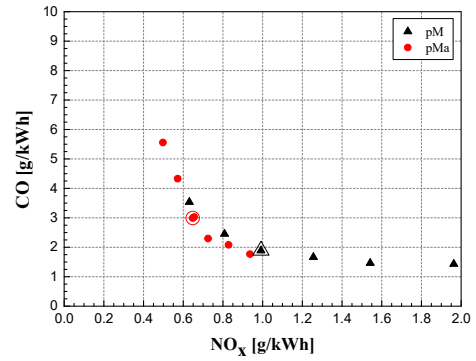


Figure 6. CO - NO_x trade-off for the *pM* and *pMa* strategies ($b_{mep}=5$ bar, $n=2000$ rpm).

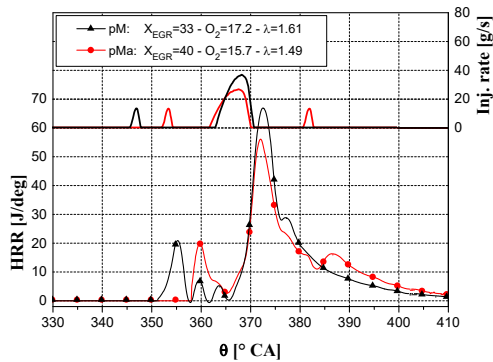


Figure 7. HRR versus θ distribution for the *pM* and *pMa* strategies ($b_{mep}=5$ bar, $n=2000$ rpm).

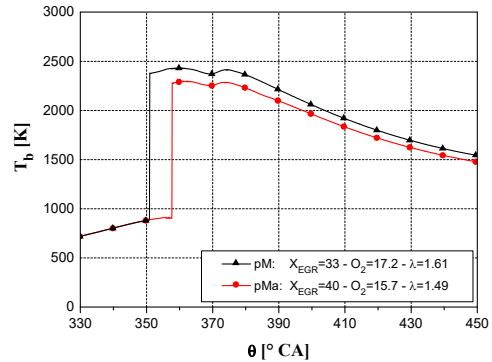


Figure 8. T_b versus θ distribution for the *pM* and *pMa* strategies ($b_{mep}=5$ bar, $n=2000$ rpm).

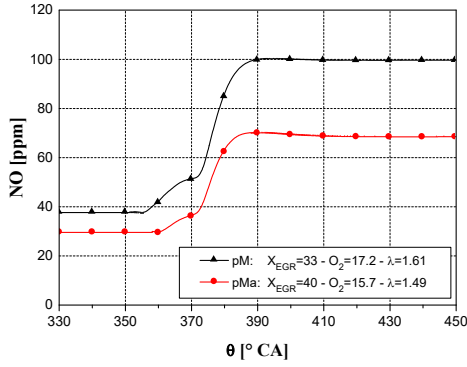


Figure 9. NO versus θ distribution for the pM and pMa strategies ($bmep=5$ bar, $n=2000$ rpm).

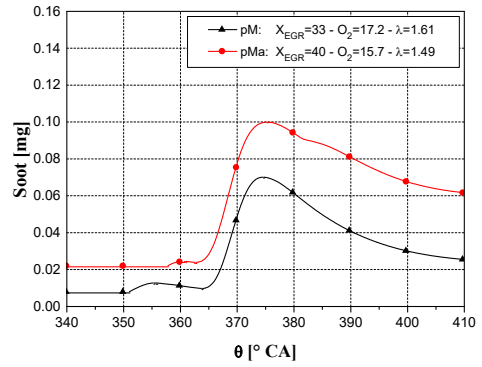


Figure 10. PM versus θ distribution for the pM and pMa strategies ($bmep=5$ bar, $n=2000$ rpm).

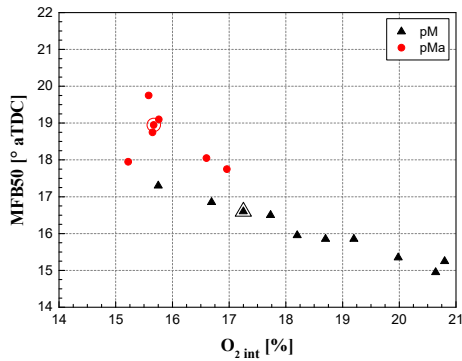


Figure 11. MFB50 as a function of X_{EGR} for the pM and pMa strategies ($bmep=5$ bar, $n=2000$ rpm).

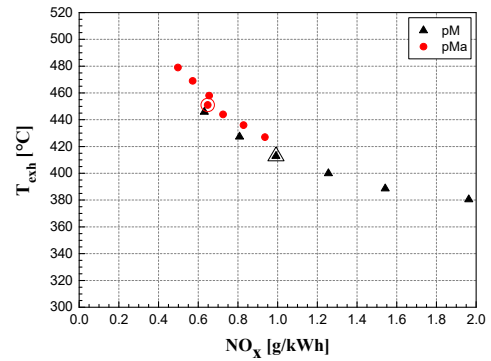


Figure 12. T_{exh} as a function of X_{EGR} for the pM and pMa strategies ($bmep=5$ bar, $n=2000$ rpm).

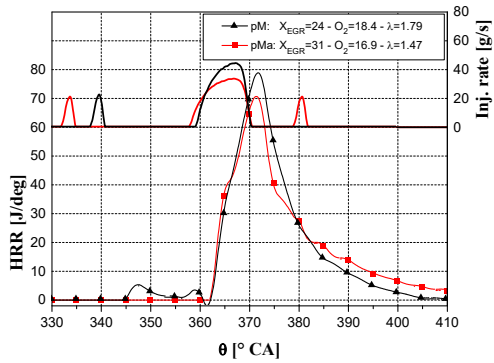


Figure 13. HRR versus θ distribution for the pM and pMa strategies ($bmep=8$ bar, $n=2500$ rpm).

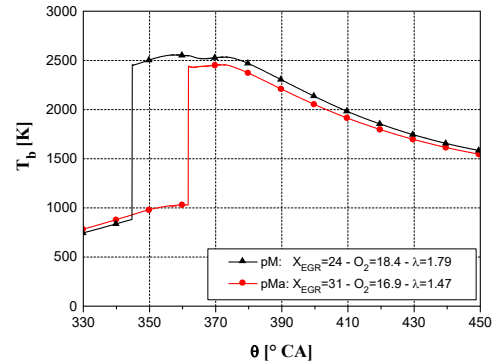


Figure 14. T_b versus θ distribution for the pM and pMa strategies ($bmep=8$ bar, $n=2500$ rpm).

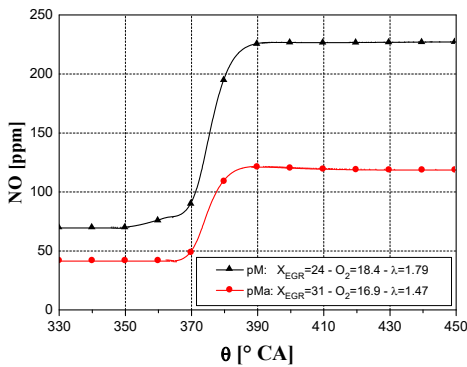


Figure 15. NO_x versus θ distribution for the pM and pMa strategies ($bmep=8$ bar, $n=2500$ rpm).

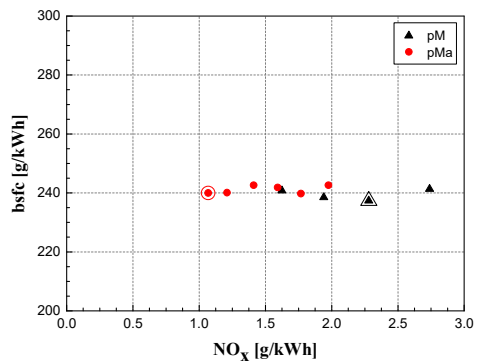


Figure 16. bsfc- NO_x trade-off for the pM and pMa strategies ($bmep=8$ bar, $n=2500$ rpm).

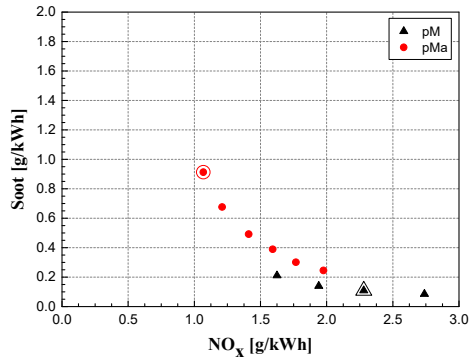


Figure 17. Soot-NO_x trade-off for the *pM* and *pMa* strategies (*bmep*=8 bar, *n*=2500 rpm).

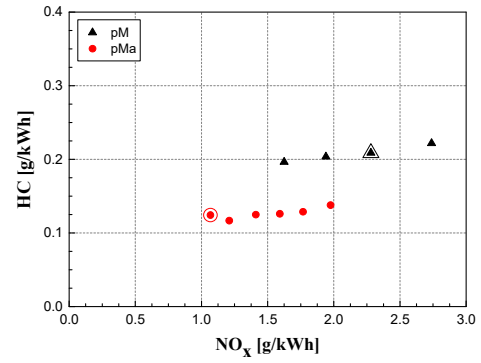


Figure 18. HC-NO_x curve for the *pM* and *pMa* strategies (*bmep*=8 bar, *n*=2500 rpm).

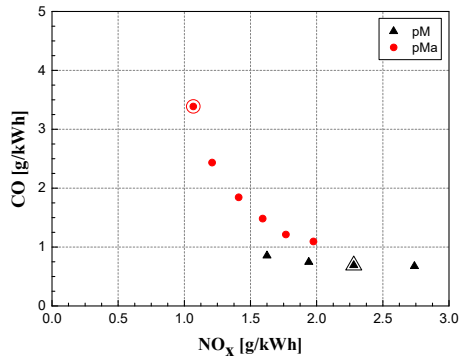


Figure 19. CO-NO_x trade-off for the *pM* and *pMa* strategies (*bmep*=8 bar, *n*=2500 rpm).

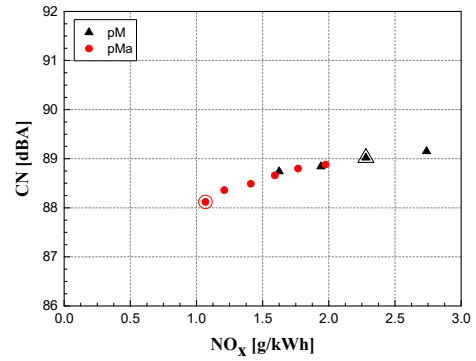


Figure 20. CN-NO_x curve for the *pM* and *pMa* strategies (*bmep*=8 bar, *n*=2500 rpm).

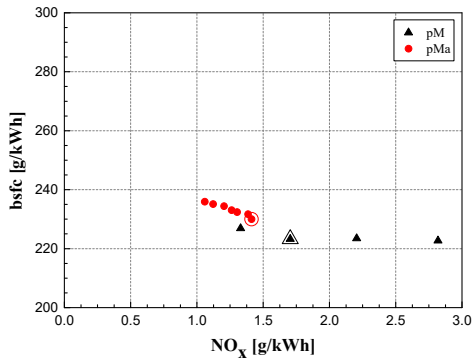


Figure 21. bsfc-NO_x trade-off for the *pM* and *pMa* strategies (*bmep*=12 bar, *n*=2750 rpm).

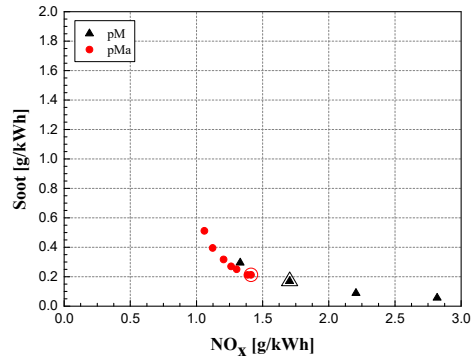


Figure 22. Soot-NO_x trade-off for the *pM* and *pMa* strategies (*bmep*=12 bar, *n*=2750 rpm).

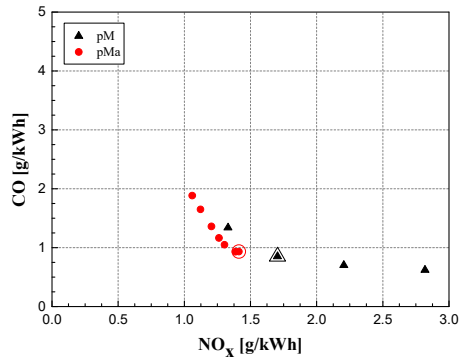


Figure 23. CO-NO_x trade-off for the *pM* and *pMa* strategies (*bmep*=12 bar, *n*=2750 rpm).

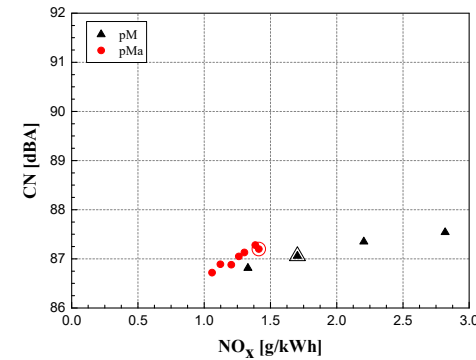


Figure 24. CN-NO_x curve for the *pM* and *pMa* strategies (*bmep*=12 bar, *n*=2750 rpm).

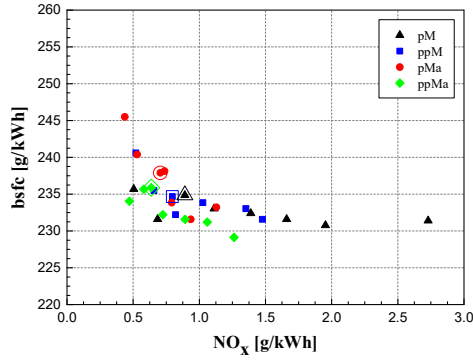


Figure 25. $bsfc$ - NO_x trade-off for the pM , ppM , pMa and $ppMa$ strategies ($bmeP=5$ bar, $n=1500$ rpm).

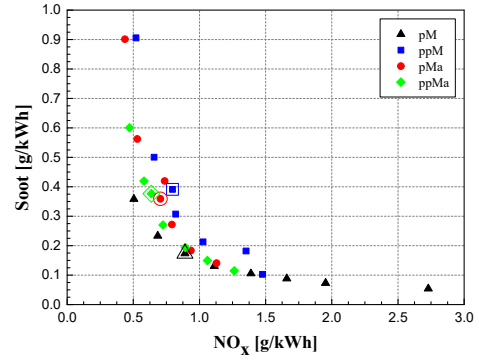


Figure 26. Soot- NO_x trade-off for the pM , ppM , pMa and $ppMa$ strategies ($bmeP=5$ bar, $n=1500$ rpm).

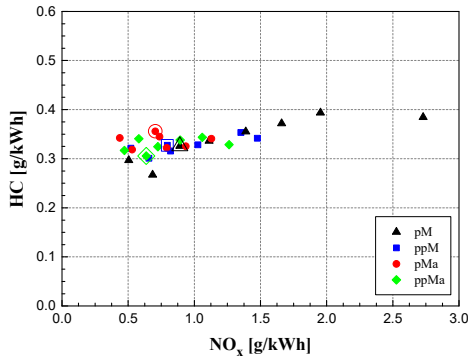


Figure 27. HC - NO_x trade-off for the pM , ppM , pMa and $ppMa$ strategies ($bmeP=5$ bar, $n=1500$ rpm).

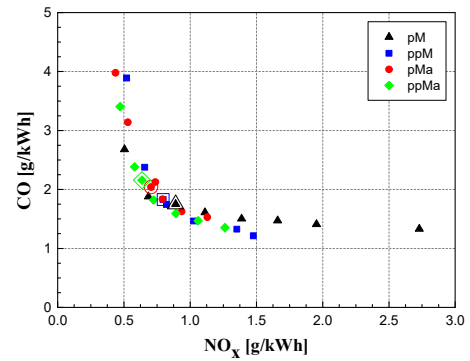


Figure 28. CO - NO_x trade-off for the pM , ppM , pMa and $ppMa$ strategies ($bmeP=5$ bar, $n=1500$ rpm).

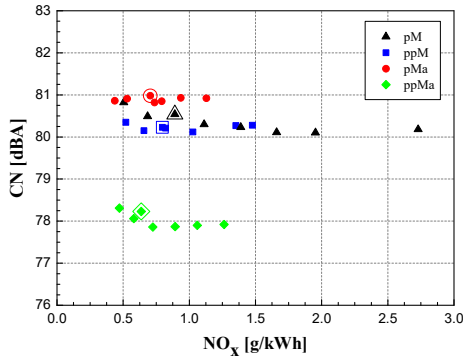


Figure 29. CN - NO_x curve for the pM , ppM , pMa and $ppMa$ strategies ($bmeP=5$ bar, $n=1500$ rpm).

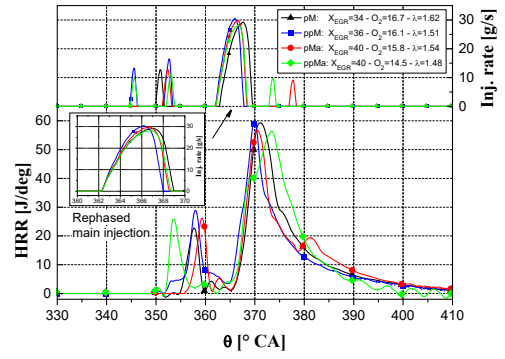


Figure 30. HRR versus θ distribution for the pM , ppM , pMa and $ppMa$ strategies ($bmeP=5$ bar, $n=1500$ rpm).

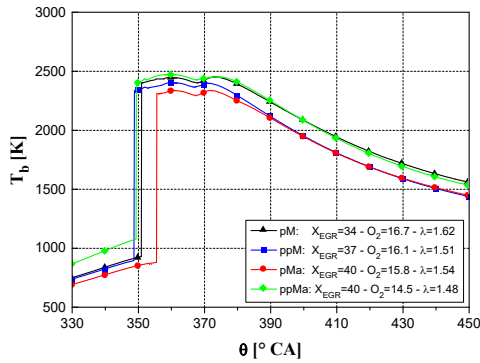


Figure 31. T_b versus θ distribution for the pM , ppM , pMa and $ppMa$ strategies ($bmeP=5$ bar, $n=1500$ rpm).

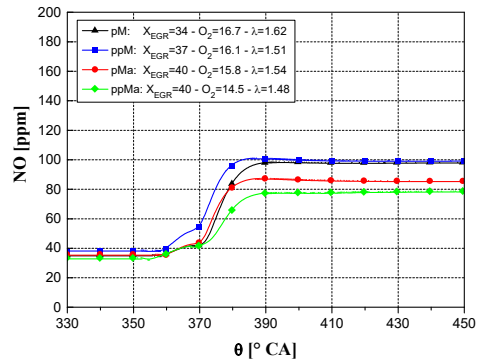


Figure 32. NO_x versus θ distribution for the pM , ppM , pMa and $ppMa$ strategies ($bmeP=5$ bar, $n=1500$ rpm).

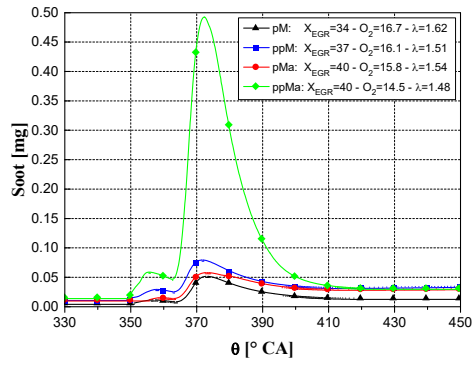


Figure 33. Soot versus θ distribution for the *pM*, *ppM*, *pMa* and *ppMa* strategies (*bme_p*=5 bar, *n*=1500 rpm).